Asian Journal of Pharmaceutical Sciences 20 (2025) 101024

Available online at www.sciencedirect.com

ScienceDirect

journal homepage: www.elsevier.com/locate/AJPS

Research Article

Microalgae-carrying nanomedicine for bioadhesive drug delivery for treating chemotherapy-induced intestinal injury

Jie Chen[a,b], *Bing Wang*[b,c,*], *Lan Shen*[a,*], *Yongzhuo Huang*[b,d,e,*]

[a] *School of Pharmacy, Shanghai University of Traditional Chinese Medicine, Shanghai 201203, China*
[b] *State Key Laboratory of Drug Research, Shanghai Institute of Materia Medica Chinese Academy of Sciences, Shanghai 201203, China*
[c] *State Key Laboratory of System Medicine for Cancer, Shanghai Cancer Institute, Renji Hospital, School of Medicine, Shanghai Jiao Tong University, Shanghai 200032, China*
[d] *Zhongshan Institute for Drug Discovery, Shanghai Institute of Materia Medica, Chinese Academy of Sciences, Zhongshan 528400, China*
[e] *NMPA Key Laboratory for Quality Research and Evaluation of Pharmaceutical Excipients, Shanghai 201203, China*

ARTICLE INFO

Article history:
Received 28 March 2024
Revised 3 December 2024
Accepted 9 December 2024
Available online 8 February 2025

Keywords:
Microalgae
Bioadhesive delivery
Chemotherapy-induced intestinal injury
Bornyl acetate
Macrophages

ABSTRACT

Gastrointestinal tract toxicity represents a serious adverse effect of chemotherapy, leading to reduced quality of life and survival. For instance, irinotecan (CPT-11) usually causes severe gastrointestinal toxicity, with a lack of effective therapeutic interventions, making treatment often unsustainable. Therefore, development of an effective and safe therapy is crucial for improving chemotherapy efficacy and the patients' quality of life. In this work, we developed a novel approach involving the helical-shaped cyanobacterium microalgae, *Spirulina platensis* (SP), to carry the bornyl acetate (BA)-loaded chitosan nanoparticles to enhance drug retention in the small intestine. We demonstrated the protection effect of BA against chemotherapy-induced intestinal injury using an epithelial cell model. In a mouse model, orally administered BA-ChNPs@SP accumulated in the small intestine and attenuated inflammation by reducing dsDNA release and oxidative stress. This was concomitant with the restoration of the intestinal barrier and modulation of the immune microenvironment. This work suggests the promise of the microalgae-carrying nanomedicine strategy for treatment of intestinal diseases, emphasizing its potential in addressing chemotherapy-induced gastrointestinal complications.

* Corresponding authors.
E-mail addresses: bwang@shsci.org (B. Wang), lanshen@shutcm.edu.cn (L. Shen), yzhuang@simm.ac.cn (Y. Huang).
Peer review under responsibility of Shenyang Pharmaceutical University.

https://doi.org/10.1016/j.ajps.2025.101024

1. Introduction

Chemotherapy confronts a formidable challenge of adverse effects. Typically, intestinal mucositis and injury are among the most debilitating side effects caused by chemotherapeutics [1]. Reportedly, approximately 90 % patients receiving chemotherapy sustain intestinal disorders related to reduced quality of life, treatment disruption, and decreased survival [2]. Intestinal epithelial cells are among the most proliferative cells that are highly sensitive to chemo drugs (e.g., 5-fluorouracil, doxorubicin, cisplatin and irinotecan) that interrupt DNA synthesis, causing apoptotic cell death and local inflammation. The common mechanisms for intestinal damage are associated with the overproduction of reactive oxygen species (ROS) and the activation of nuclear factor κ-B (NF-κB) and inflammasome, subsequently leading to increased release of proinflammatory cytokines (e.g., IL-1β and IL-6) [1]. For example, irinotecan (CPT-11) can disrupt DNA synthesis, leading to structural breakdown and killing both cancer cells and intestinal epithelial cells, exerting severe intestinal toxicity [3–5]. Severe intestinal toxicity usually results in the treatment being discontinued [6]. Currently, there is no effective prevention and therapy except for suppressing diarrhea through loperamide and octreotide [7,8]. Mitigating adverse effects while preserving anticancer efficacy is crucial for maximizing the clinical benefits of chemotherapy.

Bornyl acetate (BA), an active compound from *Amomum villosum*, has demonstrated protective effects against chemotherapy-induced intestinal mucositis by inhibiting apoptosis and modulating inflammation and oxidative stress [9]. BA exhibits various pharmacological actions, such as anti-inflammation and immunomodulation [10–13]. For example, BA regulates the immune response by inhibiting NF-κB and MAPK signaling pathways, downregulating pro-inflammatory cytokines such as TNF-α, IL-1β, and IL-6, reducing NO production, and up-regulating CD86 [12]. BA inhibits LPS-induced inflammatory responses in macrophages [13,14]. Our hypothesis posits that BA could ameliorate CPT-11-induced intestinal injury by mitigating intestinal inflammation and apoptosis. However, BA has drawbacks such as poor stability, bioavailability, and low water solubility, limiting its efficacy and application.

Oral drug administration is the predominant route for gastrointestinal disease treatment, and effective regional therapy typically requires sufficient intestinal retention and absorption. To address this challenge, we developed a bioadhesive microalgae-carrying nanomedicine strategy for enhancing the efficacy of BA. *Spirulina platensis* (SP) stands out as a promising bioadhesive carrier, widely used as a dietary supplement [15,16]. SP, characterized by its distinctive helical structure, facilitates capture by the villi, thereby extending its retention in the intestine [17]. Importantly, its negatively charged surface enables the deposition of positively charged materials through electrostatic interactions, making it ideal for carrying cationic cargos [18–21]. However, SP can only facilitate the adsorption of water-soluble drugs, and the aqueous channels and pores on its surface are only 14–16 nm in size [21,22], which makes delivering hydrophobic compounds without positive charges difficult. In this work, we proposed a combination of SP and nanoparticles, by which BA was encapsulated into cationic chitosan nanoparticles and then absorbed onto SP via charge interaction. This system (termed BA-ChNPs@SP) aimed to prolong intestinal retention to modulate CPT-11-induced intestinal injury. It is expected that BA can exhibit a reduction in cellular damage by inhibiting dsDNA release and restoring intestinal tight junctions via enhanced delivery by BA-ChNPs@SP.

2. Materials and methods

2.1. Materials

Bornyl acetate (BA) was purchased from Master Biotechnology Co., Ltd (Chengdu, China). *Spirulina platensis* (SP) was purchased from Guangyu Biological Technology Co., Ltd (Shanghai, China). Chitosan (<25 kDa, degree of deacetylation 85 %–90 %) was purchased from Yunzhou Biochemistry Co., Ltd (Qingdao, China). Sodium tripolyphosphate (TPP) and sodium carboxymethyl cellulose (CMC–Na) were purchased from Sinopharm Chemical Reagent Co., Ltd (Shanghai, China). Annexin V-FITC/PI Apoptosis Detection Kit, 1,1-dioctadecyl-3,3,3,3-tetramethylindotricarbocyaine (DiR), 7-ethyl-10-hydroxycamptothecin (SN-38), and irinotecan HCl trihydrate (CPT-11) were purchased from Meilun Biotechnology Co., Ltd (Dalian, China). 3-(4, 5-dimethylthiazol-2-yl)−2, and 5-diphenyltetrazolium bromide (MTT) were purchased from Sigma-Aldrich (Missouri, USA). RNA extraction reagent, RNA reverse transcription kit, and dsDNA assay kit were purchased from Yeasen Biotechnology Co., Ltd (Shanghai, China). Myeloperoxidase (MPO) ELISA kit was from Dakewe Biotech Co., Ltd (Shanghai, China). Superoxide dismutase (SOD), catalase (CAT), and MDA assay kit were purchased from Beyotime Biotechnology (Shanghai, China). All the cytokines were from Peprotech (Cranbury, USA). SGF and simulated intestinal fluid (SIF) were purchased from Shanghai Yuanye Bio-Technology Co., Ltd (Shanghai, China). All the flow cytometry antibodies were from Biolegend (San Diego, USA).

2.2. Cell lines and animals

IEC-6 (rat small intestine crypt epithelial) cell lines were obtained from the Type Culture Collection of the Chinese Academy of Sciences (Shanghai, China). IEC-6 cells were cultured in DMEM medium supplemented with 10 % FBS and 1 % antibiotics [streptomycin (100 U/ml)-penicillin (100 U/ml)], in an incubator with a humidified 5 % CO_2 at 37 °C. The bone marrow-derived macrophages (BMDMs) were generated by culturing the bone marrow cells from the femurs and tibias of C57BL/6 mice using a standard protocol [23]. The cells were cultured in DMEM with 20 % FBS, 1 % antibiotics [streptomycin (100 U/ml)-penicillin (100 U/ml)], and 20 ng/ml M-CSF for 4 d. C57BL/6 male mice (~6 week old) were purchased from Shanghai Laboratory Animal Center (Shanghai, China). All the animal experiments were performed following the guidelines of the Institutional Animal Care and Use Committee (IACUC)

and approved by Shanghai Institute of Materia Medica (SIMM), Chinese Academy of Sciences.

2.3. Cell viability assay

IEC-6 cells were seeded and incubated in 96-well plates (5×10^3 per well) overnight and then incubated with different concentrations of SN-38/BA/SP for 24 h. Cell viability was measured using standard MTT assay. The absorbance at 490 nm was recorded by a microreader (Multiskan, Thermo Fisher, Waltham, USA).

2.4. Quantification of dsDNA

Small intestinal lavage from 2 cm of small intestine flushed with 0.5 ml PBS. Then, small intestinal lavage and cell culture medium were centrifuged at 5,000 rpm for 5 min, and the supernatants were centrifuged again. dsDNA levels of the second supernatants were detected by using the 1× dsDNA HA assay kit according to the manufacturer's instruction.

2.5. Apoptosis assay

To analyze the ameliorative effect of BA on cell apoptosis of IEC-6 cells induced by SN-38, 1×10^5 cells were seeded to a 12-well plate, and then treated with SN-38/SN-38+BA for 24 h. After being collected and diluted by 1× Binding buffer working solution, the cell suspension (100 µl) was used for annexin V-FITC/PI Apoptosis Detection Kit and subsequently analyzed by flow cytometer (ACEA NovoCyte 3000, Agilent, Santa Clara USA).

2.6. Intestinal barrier protection and anti-inflammatory study of BA in vitro

IEC-6 cells and BMDM were seeded in 12-well plates (1×10^6 per well) and co-incubated with SN-38/SN-38+BA for 24 h, respectively. The mRNA levels of intestinal barrier markers (Claudin-1, Occludin and MUC-2) from IEC-6 and proinflammatory cytokines (IL-1β, TNF-α and IL-6) from BMDM were quantified via qPCR.

2.7. Cytokine analysis by qPCR

Total RNA in the cells and tissues was extracted with RNA extraction reagent, and then reverse transcription was performed with the RNA reverse transcription kit. Finally, the mixture of primers, cDNA, and SYBR was subjected to the CFX384 Touch Detecting System (Bio-Red, Hercules, USA) for qPCR.

2.8. Preparation characterization of BA-ChNPs@SP

Chitosan (2 mg/ml) was dissolved into acetic acid (1 %, v/v, pH 5) and the TPP was dissolved into deionized water (2 mg/ml). Afterward, 200 µl methanol with dissolved BA was added dropwise to the 5 ml chitosan solution with stirring for 30 min. Subseqently, 1 ml TPP was added dropwise to the chitosan solution at a ratio of 1:4 (w/w). The mix was stirred for 30 min. The BA-ChNPs were collected by centrifuging at 12,000 rpm to remove free chitosan, TPP, and unencapsulated BA. SP was collected by centrifugation at 3,500 rpm for 10 min and washed three times with deionized water to remove the culture medium. After resuspending in water and freezing at −20 °C for 24 h, SP powder was collected by freeze-drying for 24 h. The BA-ChNPs were resuspended in water and 50 µg/ml SP was added with gentle stirring for 10 min, followed by centrifugation at 3500 rpm for 10 min to remove free SP. The BA-ChNPs@SP are stored at 4 °C.

2.9. Characterization of BA-ChNPs@SP

The bright-field and fluorescence microscope images of SP were captured with a fluorescence microscope (DM6B fluorescence microscope, Leica, Wetzlar, Germany), and the fluorescence intensity of BA-ChNPs, SP and BA-ChNPs@SP was measured by a fluorescence spectrophotometry (HITACHI F-4600, Tokyo, Japan). As for the co-localization of SP and ChNPs, we photograph coumarin-6-stained ChNPs@SP by confocal microscopy (Olympus SpinSR10, Tokyo, Japan). The particle size, polydispersity index, and zeta potential of the BA-ChNPs, SP, and BA-ChNPs@SP were evaluated by the Malvern Zeta analyzer (Nano-ZS90, Malvern, UK). Transmission electron microscope images of BA-ChNPs were acquired using a TEM (120 kV, FEI Talos L120C, Thermo Fish Scientific, Waltham, USA). The BA was quantified by GC-FID (Agilent 7890A, Santa Clara, USA). The drug-loading capacity and encapsulation efficiency were calculated by the following formula:

$$\text{Drug loading capacity (\%)} = \frac{Weight\ of\ encapsulated\ drug}{Weight\ of\ nanoparticle} \times 100\%$$

$$\text{Encapsulation efficiency (\%)} = \frac{Weight\ of\ encapsulated\ drug}{Weight\ of\ total\ added\ drug} \times 100\%$$

2.10. Drug release and SP degradation study

The drug release behavior was evaluated by dialysis membrane (MWCO 8–14 kDa) containing BA or BA-ChNPs@SP in the SGF (pH1.2, 2 h) and consequently the SIF (pH 6.8, 6 h) which both contained 0.5 % Tween 80 on a shaker (150 rpm). BA was quantified by GC-FID. The method of GC-FID to test BA: HP-5 capillary column (30 m × 250 µm × 0.25 µm, 5 % phenyl-95 % methylene glycol as stationary phase); oven temperature 100 °C; inlet temperature 230 °C; the gas was nitrogen at a flow rate of 4.0 ml/min. The injection volume was 1 µl; the split ratio was 10:1; and the detector temperature was 250 °C. The degradation of SP was evaluated under the same condition as above. The average length of SP was estimated by ImageJ (NIH, USA).

2.11. Retention analysis of BA-ChNPs@SP

Coumarin-6 (cou-6) labeled ChNPs@SP was prepared for examining the retention ratio in SGF and SIF. Cou-6-ChNPs@SP was dispersed in SGF (2 h) and SIF (6 h) on a constant temperature shaker (37 °C, 150 rpm). The samples were taken

at different time points (0, 1, 2, 4, 6 and 8 h) and centrifuged (3,500 rpm, 10 min) to collect the Cou-6-ChNPs@SP while the detached ChNPs left in the supernatant. The fluorescence spectrophotometry was used to detect the fluorescence intensity (λ_{ex}: 450 nm, λ_{em}: 505 nm) and the retention ratio of ChNPs@SP was calculated.

The dissected small intestines from the normal mice were incubated with DiR, DiR-ChNPs, and DiR-ChNPs@SP for 1 h. After washing with PBS three times, imaging was performed with IVIS imaging system (Caliper PerkinElmer, Hopkinton, USA). To visualize the retention effect of BA-ChNPs@SP in the small intestine, male C57BL/6 mice (6 week old, $n = 3$) were administered with DiR, DiR-ChNPs, or DiR-ChNPs@SP. Different parts of the intestine tract of the mice were dissected and subjected to IVIS imaging system at different time points (4, 8 and 12 h).

2.12. *Therapeutic effect against CPT-11-induced intestinal injury model*

The mice were treated daily with 0.25 % CMC–Na, BA, BA-ChNPs and BA-ChNPs@SP at a BA dose of 10 mg/kg on Day 1, referring to the previous study of the group. Subsequently, CPT-11 was given to the mice by intraperitoneal injection at a dose of 200 mg/kg on Day 2 and 100 mg/kg on Day 4 and 6. The body weight of mice was recorded daily. The mice were sacrificed on day 10 for collection of serum, the intestinal tissue and major organs. The lengths of different parts of intestine (total intestine, small intestine, and colon) and major organs were measured. Samples were fixed in 4 % paraformaldehyde and stained with hematoxylin/eosin (H&E) and primary antibodies for pathological and immunofluorescence analysis using a standard protocol [24]. The levels of proinflammatory cytokines (IL-1β, TNF-α and IL-6) were measured via qPCR. To determine the anti-oxidative stress markers of small intestine tissue, the intestinal segments were homogenized in PBS in the ratio of 1:10 (w/v). The resulting samples were then subjected to centrifugation at 10,000 *g* for 10 min at 4 °C. The intestinal levels of redox factors were determined by SOD assay kit, CAT assay kit, MDA assay kit, and MPO assay kit.

2.13. *Flow cytometry analysis*

At the end of animal experiments, the small intestines were harvested to obtain lamina propria cells for flow cytometry according to a previous report [25]. In brief, the small intestinal tissues were incubated with intestinal epithelial digestive fluid (HBSS, 1 mM DTT, and 1 mM EDTA). The small intestinal lamina propria cells were obtained by incubation with lamina propria digestive fluid (RPMI1640, 1 mg/ml collagenase IV, 0.3 mg/ml Dnase I, and 5 % FBS) for 2 h and centrifugation. For analysis of macrophages, cell suspension was stained with CD45-APC–Cy7, F4/80-BV510, CD86-BV650, CD206-AF647 and CD80-BV421 antibodies. For examination of neutrophils and Tregs, cell suspension was stained with CD45-APC–Cy7, CD11b-AF647, Ly6G-BV605, CD3-BB770, CD4-FITC and CD25-BV421 antibodies. Afterwards, the cells were further stained with intracellular TGF-β-PE (macrophage panel) and Foxp3-PE (Treg panel) by using an intracellular staining kit (BD Biosciences, USA). The cells were measured with a flow cytometer.

2.14. *Statistical analysis*

All data were presented as mean ± SD ($n \geq 3$). Statistical analysis was performed by two-tailed Student's *t*-test or one-way ANOVA followed by Tukey's multiple comparison test and post hoc analysis. The semi-quantitative analysis of fluorescence images was implemented by Image J software (NIH, USA). Statistical significance was indicated as $^*P < 0.05$, $^*P < 0.01$ and $^*P < 0.001$; ns means not significant.

3. Results and discussion

3.1. *Protective effect of BA on intestinal injury*

CPT-11 can cause severe gastrointestinal toxicity [26,27]. Consistent with a previous report [28], intraperitoneal injection of CPT-11 in C57BL/6 mice resulted in a shortened length of the small intestine (Fig. S1A and S1B). Histopathological analysis and dsDNA levels also confirmed that small intestine injury was serious (Fig. S1C and S1D).

Rat small intestine crypt epithelial cells (IEC-6), a normal small intestinal epithelial cell line, was used as a cell model to assess the therapeutic effects of BA. SN-38 is an active metabolite of CPT-11, known for its anticancer activity [29,30]. SN-38 can cause the release of dsDNA from the intestinal epithelial cells and accumulate in the intestinal microenvironment, triggering inflammasome activation [28]. Intestinal SN-38 exposure can cause mucosa damage [31]. Therefore, SN-38, with higher water solubility than CPT-11, is often used in cellular studies [28]. Our work showed that SN-38 resulted in nearly 50 % IEC-6 cell death at 50 nM, while BA showed a high biocompatibility to IEC-6 cells (Fig. S1E and S1 G). In the SN-38-injured IEC-6 cells, BA exhibited a significant rescue effect, improving cell viability in a concentration-dependent manner (Fig. 1B). The damaging effects of SN-38 on IEC-6 cells included dsDNA release and apoptosis; BA treatment alleviated these cellular damages (Fig. 1C–1E). Notably, SN-38 also compromised the epithelial barrier functions, while BA promoted the recovery of the barrier functions, evidenced by upregulated levels of Claudin-1, Occludin, and MUC-2 (Fig. 1G).

In addition, SN-38 can induce inflammatory responses, leading to increased expression of proinflammatory cytokines (e.g., IL-1β and TNF-α) [32,33]. Our results showed that BA substantially reduced proinflammatory cytokines, including IL-1β, TNF-α, and IL-6 (Fig. 1H). The conditioned medium containing dsDNA obtained by SN-38-pretreated IEC-6 cells (Fig. 1F) showed the effects on stimulating macrophages toward M1-type polarization ($F4/80^+$ $CD80^+$ $CD86^+$), while suppressing M2 macrophages ($F4/80^+CD206^+$), indicating the induction of inflammation. BA notably increased the proportion of M2 macrophages while decreasing the proportion of M1 macrophages (Fig. 1I–1L). These results underscored the protective role of BA against SN-38-induced inflammation at the cellular level (Fig. 1A).

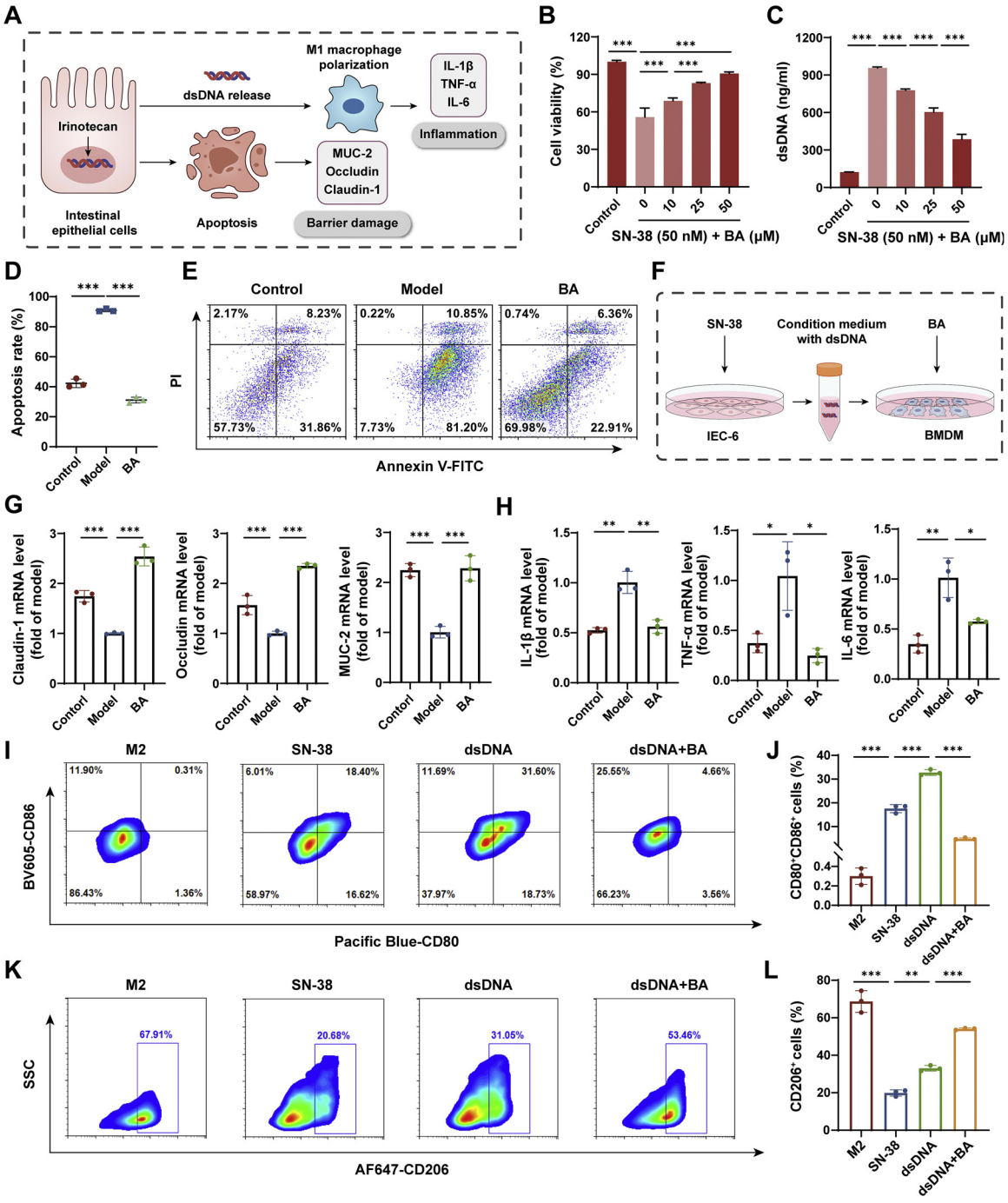

Fig. 1 – Protective and anti-inflammatory effects of BA. (A) Scheme illustration of irinotecan effect. (B) IEC-6 cell viability after treatment with SN-38 and BA. (C) dsDNA concentration in IEC-6 cells treated with SN-38 and BA. (D, E) Flow cytometry analysis of apoptosis after treatment of SN-38 and BA. (F) Experimental scheme of BMDM treatment with dsDNA-containing medium. (G) mRNA levels of Claudin-1, Occludin, and MUC-2 in IEC-6 cells measured by qPCR. (H) mRNA levels of IL-1β, TNF-α and IL-6 in BMDM measured by qPCR. (I) Representative flow cytometry plots of F4/80$^+$ CD80$^+$ CD86$^+$ M1 macrophages. (J) Percentage of M1 macrophages. (K) Representative flow cytometry plots of F4/80$^+$ CD206$^+$ M2 macrophages. (L) Percentage of M2 macrophages. Data are presented as mean ± SD (n = 3 biologically independent samples for (C–E and G–L), n = 4 biologically independent samples for (B)). Statistical analysis was evaluated with a two-tailed Student's test (G and H) and one-way ANOVA followed by Tukey's multiple comparison test and post hoc analysis (*P < 0.05, **P < 0.01, and ***P < 0.001).

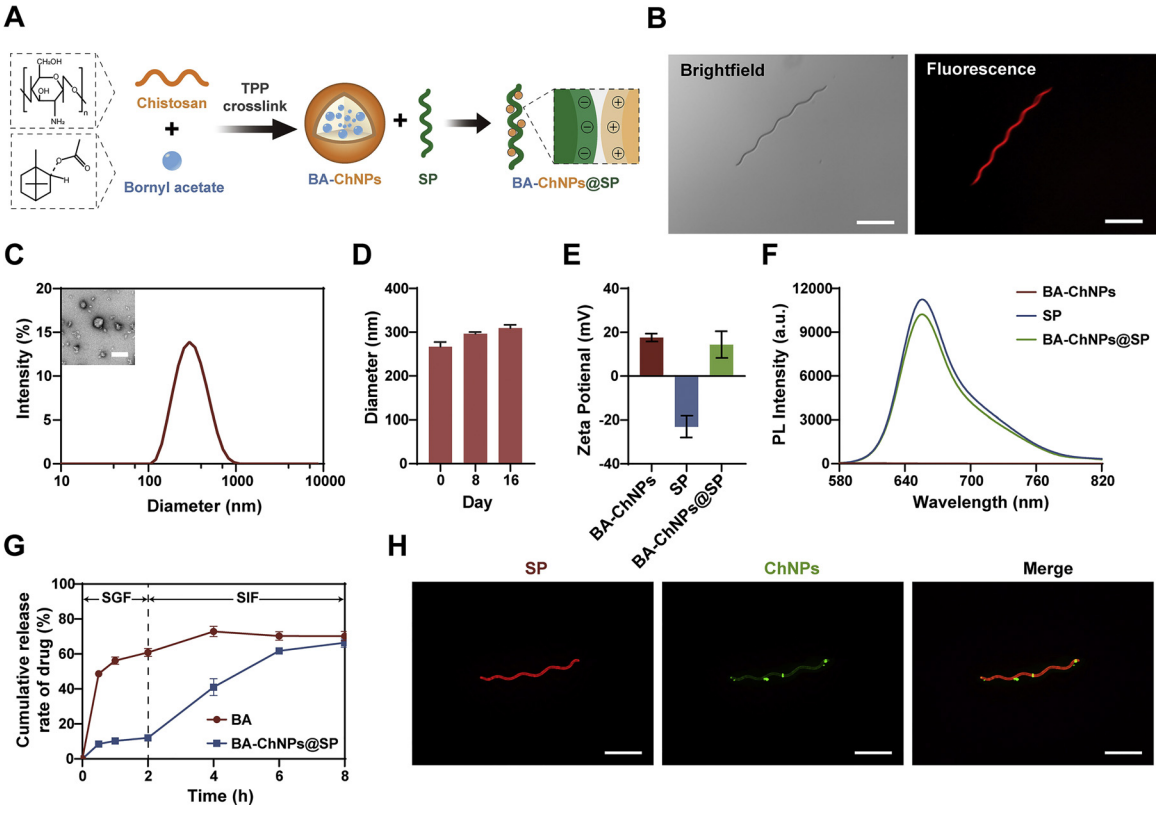

Fig. 2 – Characterization of BA-ChNPs@SP. (A) Schematic illustration of BA-ChNPs@SP preparation; (B) Brightfield and fluorescence images of SP. Scale bar: 100 μm; (C) Size distribution and TEM image of BA-ChNPs. Scale bar: 200 nm; (D) Stability of BA-ChNPs. (E) Zeta potential; (F) Fluorescence emission spectra of BA-ChNPs, SP and BA-ChNPs@SP; (G) In vitro drug release profiles in SGF and SIF; (H) Fluorescence images of ChNPs@SP. (red: SP; green: ChNPs). Scale bar: 100 μm. Data are presented as mean ± SD (*n* = 3 biologically independent samples for D, E and G).

3.2. *Characterization of BA-ChNPs@SP*

The BA-chitosan nanoparticles (BA-ChNPs) were synthesized through an ion crosslinking method (Fig. 2A). The BA-ChNPs exhibited a mean particle size of ~260 nm and a polydispersity index (PDI) of ~0.2 (Fig. 2C and Table S1). Transmission electron microscopy (TEM) revealed the morphology of the nanoparticles (Fig. 2C). The drug encapsulation efficiency was 63.8 % and drug-loading capacity of 3.7 % (Table S1). The nanoparticle loading efficiency of SP is about 58.8 % (Fig. S1J). The BA-ChNPs showed good stability over a 2-week period at 4 °C (Fig. 2D).

The BA-ChNPs were then loaded onto SP, which showed a helical shape with a length of approximately 100–200 μm (Fig. 2B). The ζ potential of BA-ChNPs@SP shifted from −23.1 to 14.3 mV after loading positively charged BA-ChNPs, indicating the successful combination of SP and BA-ChNPs (Fig. 2E). Due to the substantial presence of chlorophyll in SP, it exhibited fluorescence at λ_{em} 650 nm with λ_{ex} 550 nm (Fig. 2B). Both SP and BA-ChNPs@SP had similar fluorescence characteristics (Fig. 2F). By using coumarin 6 to label the ChNPs, confocal microscopy images showed the ChNPs (green fluorescence) localized on the surface of SP (red fluorescence) (Fig. 2H and S2A).

The cellular uptake experiments showed there was no significant difference between C6-ChNPs and C6-ChNPs@SP (Fig. S2F–S2G). This could be attributed to SP being a drug carrier with a linear structure that is not able to enter cells directly; the nanoparticles must be released from SP before they can enter the cells. In addition, the cellular biosafety of SP, BA-ChNPs, and BA-ChNPs@SP was good (Fig. S1F, S1H and S1I)

SP is stable in gastric fluid but gradually degrades in the small intestine [17]. It is well-documented that chitosan nanoparticles remain stable in gastric fluid allowing them to safely reach the intestine [34]. Consistently, our results also revealed the gastric stability of SP. The *in vitro* release study demonstrated that BA-ChNPs@SP exhibited only 12 % BA release in the SGF, but >50 % drug release in the SIF (Fig. 2G). This release profile highlights the capability of BA-ChNPs@SP to resist gastric degradation and enhance small intestinal delivery.

3.3. *The retention capacity of BA-ChNPs@SP in the small intestine*

The long-helical shape of SP renders it ready to be captured by small intestinal villi and its length is associated with the intestinal retention capacity [17]. Fig. 3B illustrates the stability of SP in SGF, without significant reduction in length, while over 6 h in SIF, SP can still maintain its long-helical shape, with a minor change in length from 80 to 60 μm (Fig. 3C). Quantitative analysis in Fig. 3C confirmed that

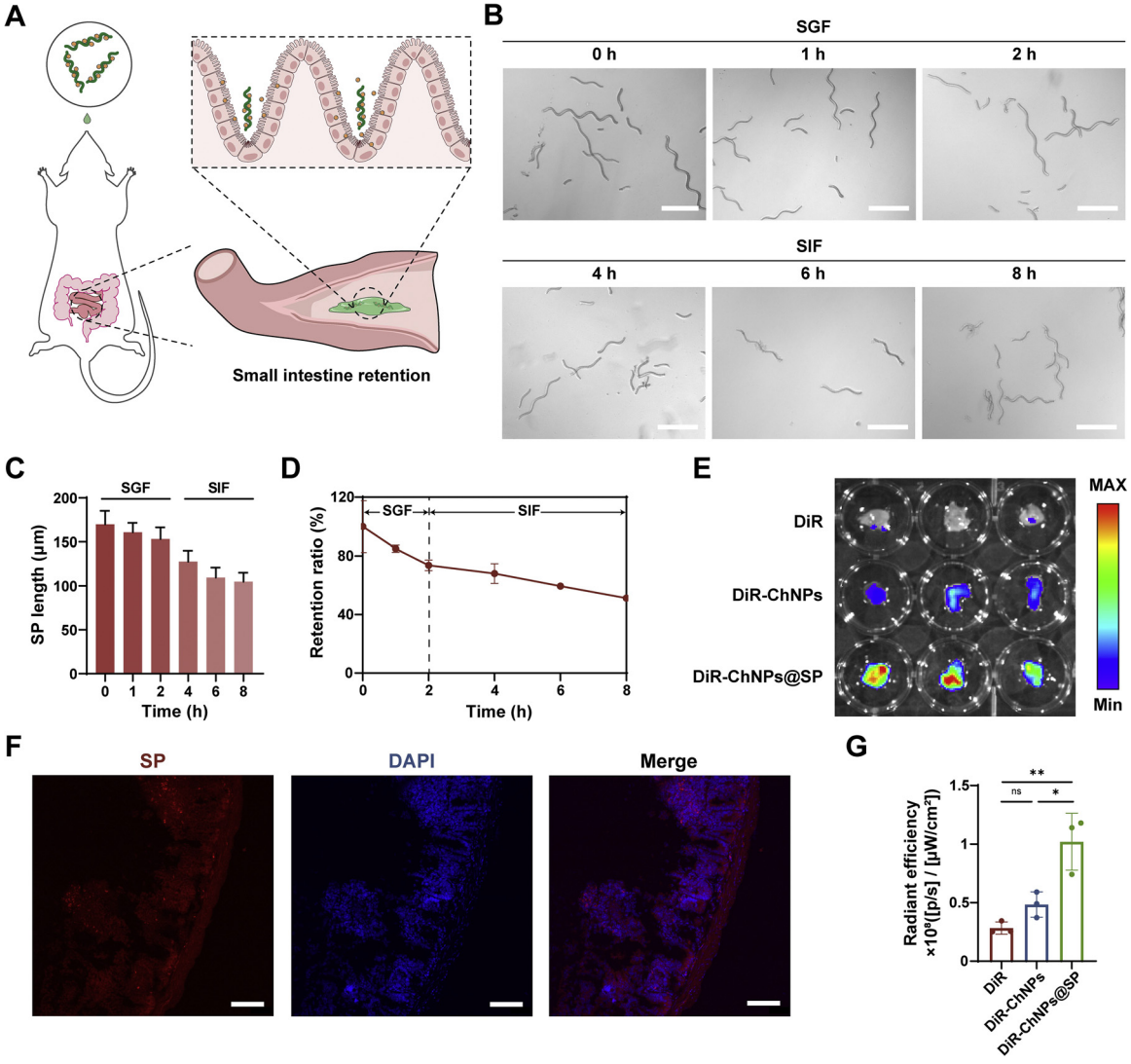

Fig. 3 – Small intestinal retention capability of BA-ChNPs@SP. (A) Scheme of targeting delivery via oral administration; (B) Bright-field images of SP in different kinds of simulated GI fluids. Scale bar: 100 μm; (C) SP lengths (indicating the stability in the simulated GI fluids); (D) Retention ratio of ChNPs@SP in SGF and SIF; (E) *Ex vivo* fluorescence images of intestines after incubation with DiR, DiR-ChNPs, and DiR-ChNPs@SP; (F) Cryosections of small intestine (DAPI staining). The red signals are SP. Scale bar: 100 μm. White arrows point to SP aggregates; (G) Region-of-interest analysis of fluorescence intensities of the intestines as shown in E. Data are presented as mean ± SD ($n = 3$ biologically independent samples for G). Statistical analysis was evaluated with one-way ANOVA followed by Tukey's multiple comparison test and post hoc analysis (*$P < 0.05$, **$P < 0.01$).

the length of the SP follows the same trend as images, demonstrating the stability of SP in the small intestine for long retention.

To investigate the cargo-carrying capacity of SP to the small intestinal villus site, we examined the binding between SP and nanoparticles in SGF and SIF. The binding percentage remained above 70 % after 2h incubation in SGF, suggesting its stability in the stomach. It exhibited 50 % after 6h incubation in SIF (Fig. 3D), indicating the sustained release of ChNPs from SP.

Furthermore, we incubated DiR-ChNPs and DiR-ChNPs@SP with the freshly dissected mouse small intestines, and after thorough washing, fluorescence imaging was carried out to evaluate bioadhesion capacity. It revealed that the DiR-ChNPs@SP groups exhibited significantly higher intestinal retention efficiency compared to DiR-ChNPs (Fig. 3E and 3G). In addition, the red fluorescence representing SP was strong at the small intestinal site, especially at the top of the villi and deep in the crypts (white arrowheads), indicating the long retention capacity of SP (Fig. 3F).

The efficiency of small intestinal targeted delivery of BA-ChNPs@SP was evaluated in C57BL/6 mice (Fig. 3A). The in vivo retention time of DiR-ChNPs@SP was prolonged to 12 h (Fig. 4A and 4C). The high fluorescence in the upper part of the abdomen at 4 h and 6 h could be due to the accumulation of DiR in the liver after being absorbed into

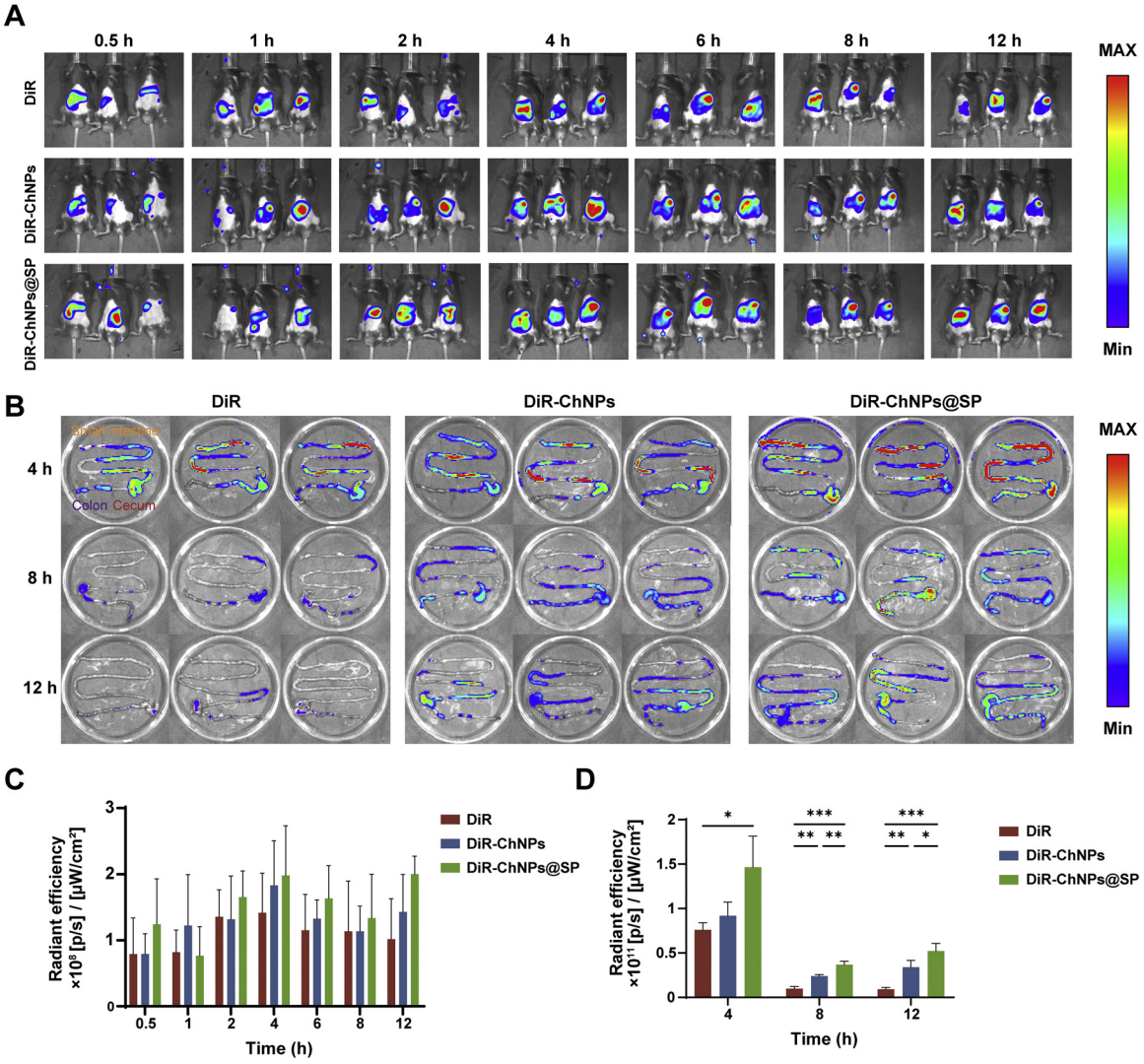

Fig. 4 – In vivo biodistribution and fluorescence imaging. (A) Fluorescence images of mice after administration; (B) *Ex vivo* fluorescence images of the intestinal tracts after the intragastrical administration; (C–D) Region-of-interest analysis fluorescence intensities as shown in A and B, respectively (Orange: small intestine; red: cecum; violet: colon). Data are presented as mean ± SD ($n = 3$ biologically independent samples). Statistical analysis was evaluated with one-way ANOVA followed by Tukey's multiple comparison test and post hoc analysis (*$P < 0.05$, **$P < 0.01$ and ***$P < 0.001$).

the blood. *Ex vivo* fluorescence imaging in different parts of the intestine, including small intestine, cecum and ileum, from the DiR-ChNPs@SP treated mice showed DiR-ChNPs@SP was still detectable at 12 h after administration, while there was none in the control groups (Fig. 4B); the quantitative data showed that the fluorescence intensity of DiR-ChNPs@SP was higher (Fig. 4D). There was no significant difference in the distribution among the three groups in other major organs (Fig. S2B–S2E). These findings suggested the excellent retention capacity of BA-ChNPs@SP in the small intestine.

3.4. *Therapeutic efficacy of BA-ChNPs@SP against CPT-11-induced small intestinal injury*

In vivo therapeutic efficacy was evaluated in a murine model with CPT-11-induced small intestinal injury. Fig. 5A illustrates the overall experimental design. CPT-11 treatment caused significant loss of body weight, while this declining trend was suppressed in the BA-ChNPs@SP treatment group (Fig. 5B). The intestine length serves as an indicator of intestinal injury. The intestinal length of the model groups was remarkably shorter than that of the normal mice, indicating significant intestinal lesions induced by CPT-11 treatment (Fig. 5C and 5D). However, treatment with BA-ChNPs@SP could prevent the shortening of intestinal length. In specific, the length of the small intestine was remarkably improved in the BA-ChNPs@SP group, indicating superior therapeutic efficacy (Fig. 5E). Histological examination of the small intestine exhibited complete loss of villi, immunocyte infiltration, and severe mucosal damage, whereas substantial improvements were found in the BA-ChNPs@SP group (Fig. 5F and 5G).

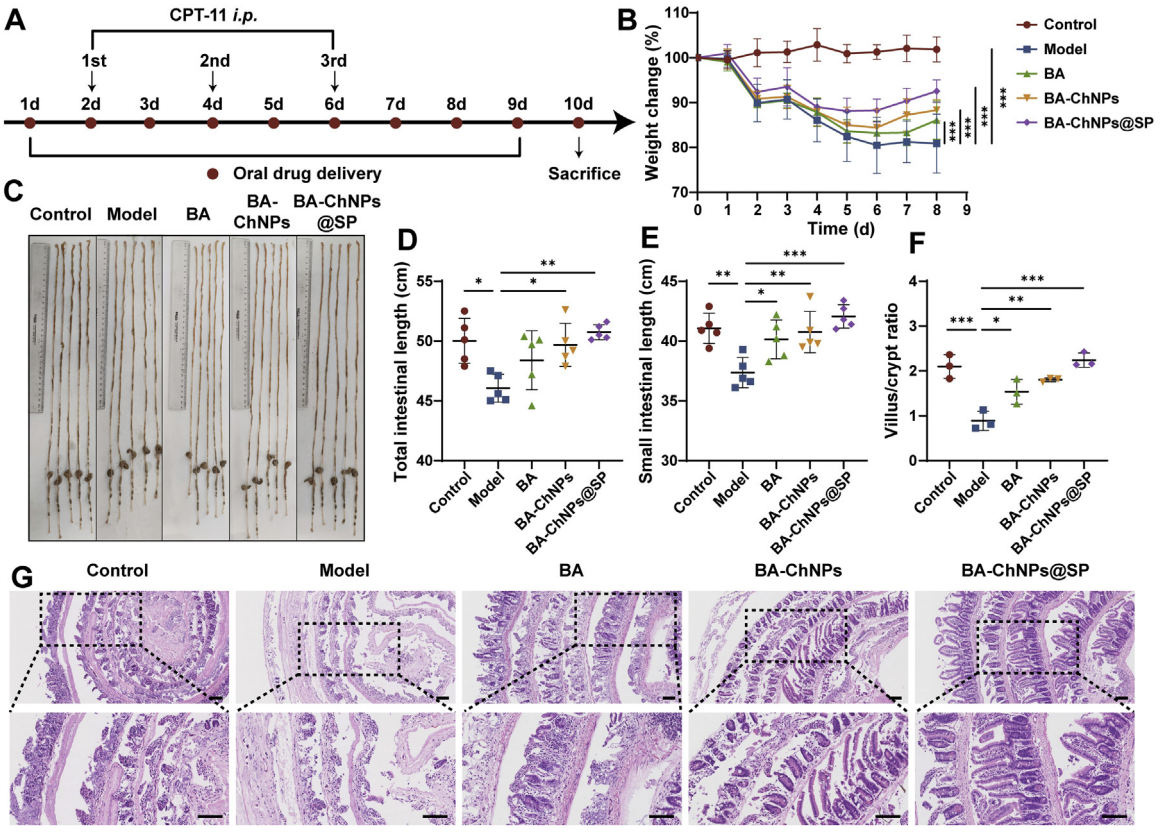

Fig. 5 – Treatment efficacy of BA-ChNPs@SP against CPT-11-induced intestinal injury. (A) Experimental procedure for treatment; (B) The body weight change of the mice; (C) Photographs of the whole intestines; The lengths of total intestine (D) and small intestine (E); (F) Villus/crypt ratio in H&E-stained small intestinal sections; (G) Representative images of H&E staining of small intestinal sections. Scale bar: 250 μm. Data are presented as mean ± SD ($n = 5$ biologically independent samples for B–E, $n = 3$ biologically independent samples for F). Statistical analysis was evaluated with one-way ANOVA and Tukey's multiple comparison test and post hoc analysis (*$P < 0.05$, **$P < 0.01$ and ***$P < 0.001$).

TUNEL staining of the small intestinal tissues showed that the BA-ChNPs@SP group markedly alleviated apoptosis compared to the BA and BA-ChNPs groups, emphasizing the critical role of SP retention in the small intestine (Fig. 6A and 6D). Immunofluorescence staining of ZO-1 and MUC-2, markers for the small intestine epithelial barrier, revealed that CPT-11 treatment significantly reduced the expression of ZO-1 and MUC-2 in the small intestine (Fig. 6B–6D). These proteins are crucial for maintaining the structure and function of the intestinal epithelium as well as the integrity of the intestinal barrier. Importantly, the intestinal barrier function was repaired by treatment with BA-ChNPs@SP, as evidenced by the upregulation of the tight-junction protein ZO-1.

Moreover, BA-ChNPs@SP significantly reduced CPT-11-induced dsDNA release (Fig. 6E) and mitigated inflammatory responses by decreasing the production of proinflammatory cytokines, including TNF-α, IL-1β and IL-6 (Fig. 6F–6H).

Furthermore, oxidative stress was determined. SOD scavenges superoxide radicals and plays a crucial role against free radical damage and inflammation. SOD levels in CPT-11-treated mice were notably reduced, but treatment of BA-ChNPs@SP upregulated SOD levels (Fig. 6I). CAT is an antioxidant enzyme that mitigates oxidative stress via scavenging hydrogen peroxide. Our results showed the effect of BA-ChNPs@SP on CAT upregulation (Fig. 6J). Malondialdehyde (MDA) is a secondary product of lipid peroxidation. CPT-11 triggered an increase in MDA levels, which were, however, decreased after BA-ChNPs@SP treatment (Fig. 6K). It suggested that BA-ChNPs@SP could inhibit lipid peroxidation process. MPO, secreted by activated leukocytes, catalyzes the formation of reactive intermediates and promotes lipid peroxidation. Similarly, MPO levels in CPT-11 treated mice increased sharply, but showed no obvious differences from normal levels (Fig. 6L) after treatment with BA-ChNPs@SP.

Taken together, our results demonstrated that BA-ChNPs@SP treatment could successfully alleviate CPT-11-induced intestinal injury.

3.5. *Modulatory effect of BA-ChNPs@SP on immune microenvironment in the small intestine*

CPT-11-mediated dsDNA release elicits immunogenic responses [35,36]. We analyzed the small intestinal immune cells by flow cytometry. In the BA-ChNPs@SP

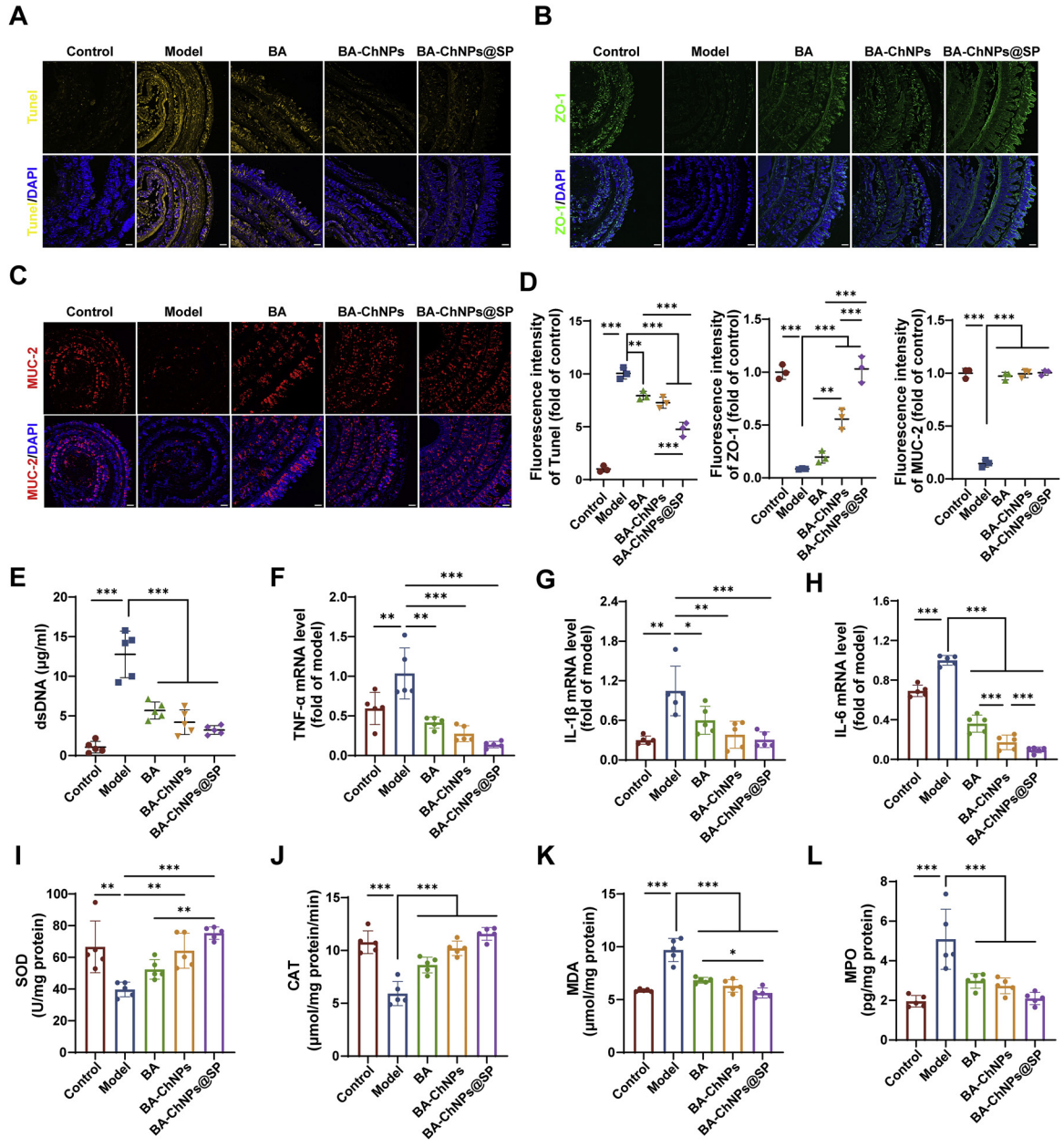

Fig. 6 – Repairing effect on the small intestinal epithelial barrier. (A) Representative TUNEL staining images of the small intestine sections; Representative immunofluorescence staining images of the small intestine sections to indicate the expression of (B) ZO-1 and (C) MUC-2. Scale bar: 100 μm; (D) Relative fluorescence intensity of the small intestine sections as shown in A–C; (E) Concentration of dsDNA in small intestinal lavage fluid; (F–H) The mRNA levels of TNF-α, IL-1β, and IL-6 in the small intestine tissues measured by qPCR; (I) SOD activity, (J) CAT activity and (K) MDA levels in the small intestines; (L) The MPO activity in the small intestine tissues measured by ELISA. Data are presented as mean ± SD ($n = 3$ biologically independent samples for D, $n = 5$ biologically independent samples for F–L). Statistical analysis by one-way ANOVA followed by Tukey's multiple comparison test and post hoc analysis (*$P < 0.05$, **$P < 0.01$ and ***$P < 0.001$).

group, there was a significant decrease in the proportion of M1 macrophages ($CD45^+CD11b^+F4/80^+CD80^+CD86^+$), showing 2.4 %, compared to 24.2 % observed in the model group (Fig. 7A and 7E). Conversely, the proportion of M2 macrophages ($CD45^+CD11b^+F4/80^+CD206^+TGF\text{-}\beta^+$) increased 4-fold compared with the model group (Fig. 7B and 7F). These results indicated that BA-ChNPs@SP promoted the transition of macrophages from M1 to M2 phenotype, thereby mitigating intestinal inflammation.

Moreover, neutrophils, which are pivotal in inflammation, are among the first leukocytes recruited to inflammatory sites [37]. Regulatory T (Treg) cells play a crucial role in curbing intestinal inflammatory responses and autoimmune reactions at the mucosal interface [38,39]. Following BA-

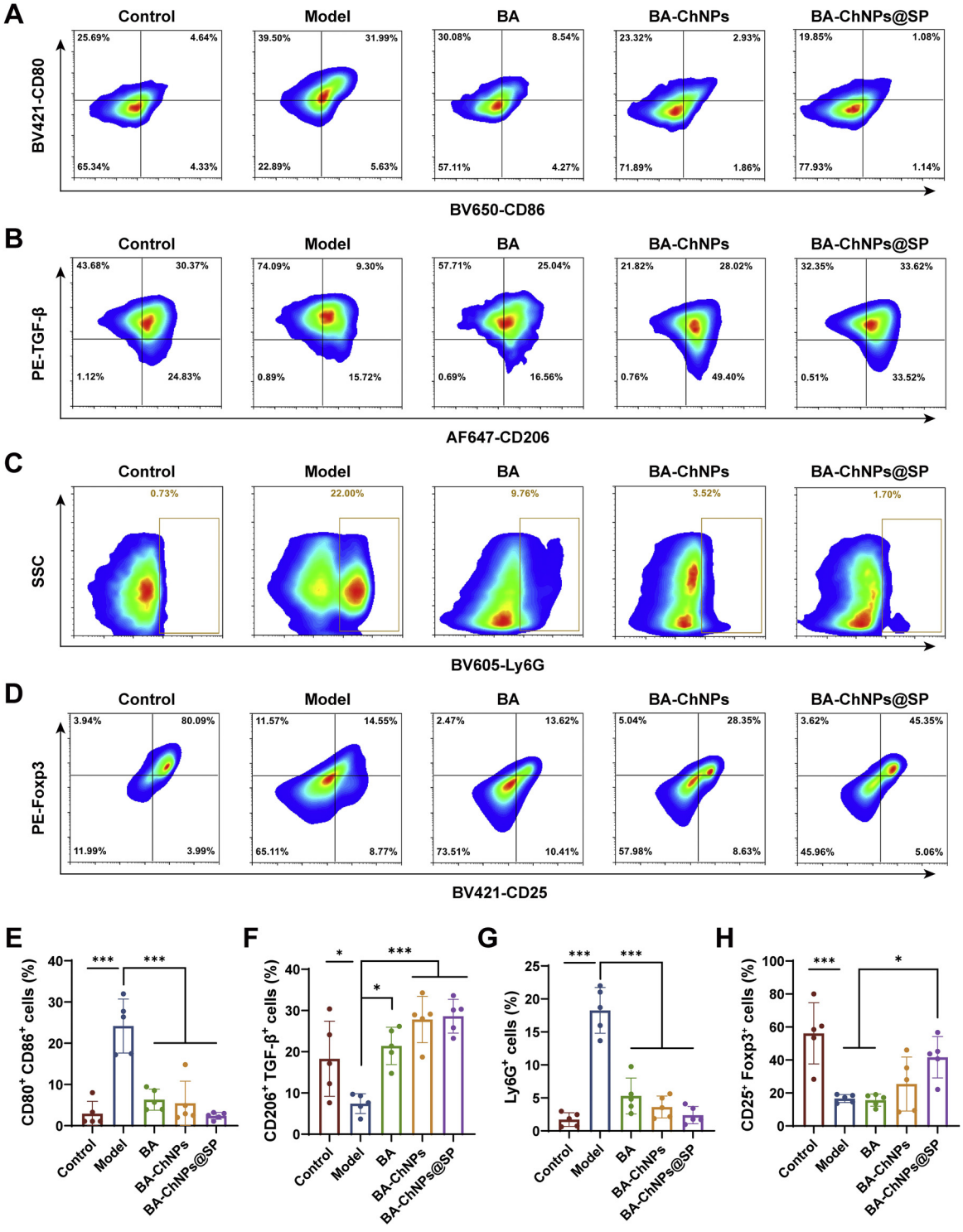

Fig. 7 – Remodeling the inflammatory microenvironment in the small intestinal tissues. Representative flow cytometry plots of (A) $CD45^+CD11b^+F4/80^+CD80^+CD86^+$ M1 macrophages, (B) $CD45^+CD11b^+F4/80^+CD206^+TGF\text{-}\beta^+$ M2 macrophages, (C) $CD45^+CD11b^+Ly6G^+$ neutrophils, and (D) $CD45^+CD3^+CD4^+CD25^+Foxp3^+$ Treg cells in the small intestines. Percentage of (E) M1 macrophages, (F) M2 macrophages, (G) neutrophils, and (H) Treg cells in the small intestines. Data are presented as mean ± SD ($n = 5$ biologically independent samples for E–H). Statistical analysis was evaluated with one-way ANOVA followed by Tukey's multiple comparison test and post hoc analysis (*$P < 0.05$, **$P < 0.01$ and ***$P < 0.001$).

ChNPs@SP treatment, there was a decrease in the proportion of neutrophils ($CD45^+CD11b^+Ly6G^+$) (Fig. 7C and G), while the proportion of Treg cells ($CD45^+CD3^+CD4^+CD25^+Foxp3^+$) was notably elevated (Fig. 7D and H). These results revealed the effective modulation of the small intestinal immune microenvironment by BA-ChNPs@SP, highlighting the potential for small intestinal protection.

3.6. *Biosafety of BA-ChNPs@SP*

To address safety concerns, we conducted histological examinations of organ tissue sections stained with H&E and calculated organ coefficients. The results revealed that major organs (e.g., heart, liver, spleen, lung, and kidney) maintained normal structures without any obvious inflammatory lesions or damage. Furthermore, there were no differences in the organ coefficients among the tested groups (Fig. S3A and S3B). In addition, the liver and kidney function parameters, including alanine aminotransferase (ALT), aspartate aminotransferase (AST), creatinine (CRE), and blood urea nitrogen (BUN), showed no significant difference (Fig. S3C–S3F). These results suggested the biosafety of BA-ChNPs@SP for in vivo application.

3.7. *Discussion*

The mechanism of CPT-11-induced intestinal injury is not fully understood. CPT-11-mediated dsDNA breaks impede DNA replication and induce apoptosis [40–43], resulting in histopathologic changes [44]. Furthermore, the released dsDNA acts as a damage-associated molecular pattern (DAMP), triggering innate immune responses [45], as well as activating inflammatory responses through cGAS-STING pathway [46,47]. There are no effective drugs available yet for specifically treating chemotherapy-induced intestinal injury. Our work revealed the therapeutic potential of an active compound (BA) from a Chinese herb that has been well-documented for treating gastrointestinal diseases. To address the intestine-specific delivery barrier for such water-insoluble compound, we developed a promising strategy of combination of SP carrier and chitosan nanoparticles and thus achieved enhanced small intestinal delivery.

While previous studies have explored the medicinal potential of microalgae or the concept of microalgae vaccines [15,16], the application of microalgae in drug delivery, particularly in treating intestinal diseases, has been rare. Strategies such modifying magnetic nanoparticles on the surface of microalgae for magnetic field-guiding target [48], or using microalgae's aqueous channels to load small molecules [21,22] have been explored. However, the utilization feasibility of oral delivery for water-insoluble drugs was not known. Therefore, combining microalgae with nanoparticles in drug delivery strategies presents a promising avenue with broader applications.

SP has been demonstrated protective effects on both the stomach and intestines at a high SP dose of 1,500 mg/kg for 28 d in rats and 160 mg/kg for 7 d in mice to yield an effective efficacy [49,50]. In our work, the SP dose is 15.6 mg/kg for 8 d, which is far below the therapeutic dose of SP. Therefore, SP may only serve as a carrier in this application.

4. Conclusion

To address the complexity of the intestinal environment, we employed a strategy involving microalgae SP to effectively orally deliver the BA-loaded chitosan nanoparticles. BA-ChNPs@SP demonstrated remarkable small intestinal retention capability and significantly enhanced local drug exposure. The long-helical shape of SP facilitated adhesion to villi, thereby increasing drug release in the small intestine. Oral administration of BA-ChNPs@SP exerted protective effects on the intestine and exhibited anti-inflammation ability, noticeably reducing oxidative stress. Moreover, BA-ChNPs@SP demonstrated good biosafety and had an advantage of a straightforward process for formulation preparation. Therefore, the microalgae-nanomedicine treatment can serve as a promising BA-based therapeutic strategy for the management of intestinal diseases.

Conflicts of interest

The authors report no conflicts of interest. The authors alone are responsible for the content and writing of this article.

Acknowledgments

We are thankful to the National Key Research and Development Program of China (2022YFE0203600, China), NFSC (81925035, 82341232), Program of Shanghai Committee of Science and Technology (21ZR1475200, China), Department of Science and Technology of Guangdong Province (High-Level R&D and Innovative Research Institute 2021B0909050003), and SciTech Projects of Zhongshan (CXTD2022011, LJ2021001). We are thankful for the support from the Molecular Imaging Center, TEM, and Flow Cytometry Facility at SIMM, CAS. In addition, we thank the staff members of the Large-scale Protein Preparation System at the National Facility for Protein Science in Shanghai (NFPS), Shanghai Advanced Research Institute, Chinese Academy of Science, China for providing the Electron Microscopy System and Flow cytometry technical support and assistance in data collection and analysis.

Supplementary materials

Supplementary material associated with this article can be found, in the online version, at doi:10.1016/j.ajps.2025.101024. The figures and tables with "S" before the serial number are included in the Supplementary data.

References

[1] Sougiannis AT, VanderVeen BN, Davis JM, Fan D, Murphy EA. Understanding chemotherapy-induced intestinal mucositis and strategies to improve gut resilience. Am J Physiol Gastrointest Liver Physiol 2021;320(5):G712–9.

[2] Keefe DM, Elting LS, Nguyen HT, Grunberg SM, Aprile G, Bonaventura A, et al. Risk and outcomes of chemotherapy-induced diarrhea (CID) among patients with colorectal cancer receiving multi-cycle chemotherapy. Cancer Chemother Pharmacol 2014;74(4):675–80.
[3] Pizzolato JF, Saltz LB. The camptothecins. Lancet 2003;361(9376):2235–42.
[4] Elad S, Cheng KKF, Lalla RV, Yarom N, Hong C, Logan RM, et al. MASCC/ISOO clinical practice guidelines for the management of mucositis secondary to cancer therapy. Cancer 2020;126(19):4423–31.
[5] Carlotto A, Hogsett VL, Maiorini EM, Razulis JG, Sonis ST. The economic burden of toxicities associated with cancer treatment: review of the literature and analysis of nausea and vomiting, diarrhoea, oral mucositis and fatigue. PharmacoEcon 2013;31(9):753–66.
[6] Mego M, Chovanec J, Vochyanova-Andrezalova I, Konkolovsky P, Mikulova M, Reckova M, et al. Prevention of irinotecan induced diarrhea by probiotics: a randomized double blind, placebo controlled pilot study. Complement Ther Med 2015;23(3):356–62.
[7] Abigerges D, Armand JP, Chabot GG, Da Costa L, Fadel E, Cote C, et al. Irinotecan (CPT-11) high-dose escalation using intensive high-dose loperamide to control diarrhea. J Natl Cancer Inst 1994;86(6):446–9.
[8] Zidan J, Haim N, Beny A, Stein M, Gez E, Kuten A. Octreotide in the treatment of severe chemotherapy-induced diarrhea. Ann Oncol 2001;12(2):227–9.
[9] Zhang T, Lu SH, Bi Q, Liang L, Wang YF, Yang XX, et al. Volatile oil from amomi fuctus attenuates 5-fluorouracil-induced intestinal mucositis. Front Pharmacol 2017;8:786.
[10] Begum A, Sandhya S, Shaffath Ali S, Vinod KR, Reddy S, Banji D. An in-depth review on the medicinal flora rosmarinus officinalis (Lamiaceae). Acta Sci Pol Technol Aliment 2013;12(1):61–73.
[11] Lee JI, Choi JH, Kwon TW, Jo HS, Kim DG, Ko SG, et al. Neuroprotective effects of bornyl acetate on experimental autoimmune encephalomyelitis via anti-inflammatory effects and maintaining blood-brain-barrier integrity. Phytomedicine 2023;112:154569.
[12] Zhao ZJ, Sun YL, Ruan XF. Bornyl acetate: a promising agent in phytomedicine for inflammation and immune modulation. Phytomedicine 2023;114:154781.
[13] Yang L, Liu J, Li Y, Qi G. Bornyl acetate suppresses ox-LDL-induced attachment of THP-1 monocytes to endothelial cells. Biomed Pharmacother 2018;103:234–9.
[14] Chen N, Sun G, Yuan X, Hou J, Wu Q, Soromou LW, et al. Inhibition of lung inflammatory responses by bornyl acetate is correlated with regulation of myeloperoxidase activity. J Surg Res 2014;186(1):436–45.
[15] Rosales-Mendoza S, Angulo C, Meza B. Food-grade organisms as vaccine biofactories and oral delivery vehicles. Trends Biotechnol 2016;34(2):124–36.
[16] Wu Q, Liu L, Miron A, Klímová B, Wan D, Kuča K. The antioxidant, immunomodulatory, and anti-inflammatory activities of Spirulina: an overview. Arch Toxicol 2016;90(8):1817–40.
[17] Zhong D, Zhang D, Chen W, He J, Ren C, Zhang X, et al. Orally deliverable strategy based on microalgal biomass for intestinal disease treatment. Sci Adv 2021;7(48):eabi9265.
[18] Park JH, Yang SH, Lee J, Ko EH, Hong D, Choi IS. Nanocoating of single cells: from maintenance of cell viability to manipulation of cellular activities. Adv Mater 2014;26(13):2001–10.
[19] Akolpoglu MB, Dogan NO, Bozuyuk U, Ceylan H, Kizilel S, Sitti M. High-yield production of biohybrid microalgae for on-demand cargo delivery. Adv Sci 2020;7(16):2001256.
[20] Park BW, Zhuang J, Yasa O, Sitti M. Multifunctional bacteria-driven microswimmers for targeted active drug delivery. ACS Nano 2017;11(9):8910–23.
[21] Zhong D, Zhang D, Xie T, Zhou M. Biodegradable microalgae-based carriers for targeted delivery and imaging-guided therapy toward lung metastasis of breast cancer. Small 2020;16(20):e2000819.
[22] Wang X, Cai J, Sun L, Zhang S, Gong D, Li X, et al. Facile fabrication of magnetic microrobots based on spirulina templates for targeted delivery and synergistic Chemo-photothermal therapy. ACS Appl Mater Interfaces 2019;11(5):4745–56.
[23] Zhao P, Zhang J, Wu A, Zhang M, Zhao Y, Tang Y, et al. Biomimetic codelivery overcomes osimertinib-resistant NSCLC and brain metastasis via macrophage-mediated innate immunity. J Control Release 2021;329:1249–61.
[24] Zhou J, Li M, Chen Q, Li X, Chen L, Dong Z, et al. Programmable probiotics modulate inflammation and gut microbiota for inflammatory bowel disease treatment after effective oral delivery. Nat Commun 2022;13(1):3432.
[25] Neudecker V, Haneklaus M, Jensen O, Khailova L, Masterson JC, Tye H, et al. Myeloid-derived miR-223 regulates intestinal inflammation via repression of the NLRP3 inflammasome. J Exp Med 2017;214(6):1737–52.
[26] Xue H, Field CJ, Sawyer MB, Dieleman LA, Baracos VE. Prophylactic ciprofloxacin treatment prevented high mortality, and modified systemic and intestinal immune function in tumour-bearing rats receiving dose-intensive CPT-11 chemotherapy. Br J Cancer 2009;100(10):1581–8.
[27] Wang D, Li D, Zhang Y, Chen J, Zhang Y, Liao C, et al. Functional metabolomics reveal the role of AHR/GPR35 mediated kynurenic acid gradient sensing in chemotherapy-induced intestinal damage. Acta Pharm Sin B 2021;11(3):763–80.
[28] Lian Q, Xu J, Yan S, Huang M, Ding H, Sun X, et al. Chemotherapy-induced intestinal inflammatory responses are mediated by exosome secretion of double-strand DNA via AIM2 inflammasome activation. Cell Res 2017;27(6):784–800.
[29] Karas S, Etheridge AS, Tsakalozou E, Ramírez J, Cecchin E, van Schaik RHN, et al. Optimal sampling strategies for irinotecan (CPT-11) and its active metabolite (SN-38) in cancer patients. Aaps j 2020;22(3):59.
[30] Lavelle F, Bissery MC, André S, Roquet F, Riou JF. Preclinical evaluation of CPT-11 and its active metabolite SN-38. Semin Oncol 1996;23(1 Suppl 3):11–20.
[31] Sun R, Zhu L, Li L, Song W, Gong X, Qi X, et al. Irinotecan-mediated diarrhea is mainly correlated with intestinal exposure to SN-38: critical role of gut ugt. Toxicol Appl Pharmacol 2020;398:115032.
[32] Zhang Q, Zhang F, Li S, Liu R, Jin T, Dou Y, et al. A multifunctional nanotherapy for targeted treatment of colon cancer by simultaneously regulating tumor microenvironment. Theranostics 2019;9(13):3732–53.
[33] Gençosman S, Ceylanlı D, Şehirli A, Teralı K, Bölükbaşı F, Çetinel Ş, et al. Investigation of the possible protective effect of N-acetylcysteine (NAC) against irinotecan (CPT-11)-induced toxicity in rats. Antioxidants (Basel) 2022;11(11):2219.
[34] Wu D, Zhu L, Li Y, Wang H, Xu S, Zhang X, et al. Superparamagnetic chitosan nanocomplexes for colorectal tumor-targeted delivery of irinotecan. Int J Pharm 2020;584:119394.
[35] Garg AD, Krysko DV, Vandenabeele P, Agostinis P. DAMPs and PDT-mediated photo-oxidative stress: exploring the unknown. Photochem Photobiol Sci 2011;10(5):670–80.
[36] Ahn J, Gutman D, Saijo S, Barber GN. STING manifests self DNA-dependent inflammatory disease. Proc Natl Acad Sci USA 2012;109(47):19386–91.

[37] Kolaczkowska E, Kubes P. Neutrophil recruitment and function in health and inflammation. Nat Rev Immunol 2013;13(3):159–75.
[38] Arpaia N, Campbell C, Fan X, Dikiy S, van der Veeken J, deRoos P, et al. Metabolites produced by commensal bacteria promote peripheral regulatory T-cell generation. Nature 2013;504(7480):451–5.
[39] Josefowicz SZ, Niec RE, Kim HY, Treuting P, Chinen T, Zheng Y, et al. Extrathymically generated regulatory T cells control mucosal TH2 inflammation. Nature 2012;482(7385):395–9.
[40] Shinohara H, Killion JJ, Kuniyasu H, Kumar R, Fidler IJ. Prevention of intestinal toxic effects and intensification of irinotecan's therapeutic efficacy against murine colon cancer liver metastases by oral administration of the lipopeptide JBT 3002. Clin Cancer Res 1998;4(9):2053–63.
[41] Juang V, Chang CH, Wang CS, Wang HE, Lo YL. pH-responsive PEG-shedding and targeting peptide-modified nanoparticles for dual-delivery of irinotecan and microRNA to enhance tumor-specific therapy. Small 2019;15(49):e1903296.
[42] Keefe DM, Brealey J, Goland GJ, Cummins AG. Chemotherapy for cancer causes apoptosis that precedes hypoplasia in crypts of the small intestine in humans. Gut 2000;47(5):632–7.
[43] Alagoz M, Gilbert DC, El-Khamisy S, Chalmers AJ. DNA repair and resistance to topoisomerase I inhibitors: mechanisms, biomarkers and therapeutic targets. Curr Med Chem 2012;19(23):3874–85.
[44] Ikuno N, Soda H, Watanabe M, Irinotecan Oka M. CPT-11) and characteristic mucosal changes in the mouse ileum and cecum. J Natl Cancer Inst 1995;87(24):1876–83.
[45] Krysko DV, Garg AD, Kaczmarek A, Krysko O, Agostinis P, Vandenabeele P. Immunogenic cell death and DAMPs in cancer therapy. Nat Rev Cancer 2012;12(12):860–75.
[46] Wang Y, Wei B, Wang D, Wu J, Gao J, Zhong H, et al. DNA damage repair promotion in colonic epithelial cells by andrographolide downregulated cGAS–STING pathway activation and contributed to the relief of CPT-11-induced intestinal mucositis. Acta Pharm Sin B 2022;12(1):262–73.
[47] Ahn J, Barber GN. Self-DNA, STING-dependent signaling and the origins of autoinflammatory disease. Curr Opin Immunol 2014;31:121–6.
[48] Yasa O, Erkoc P, Alapan Y, Sitti M. Microalga-powered microswimmers toward active cargo delivery. Adv Mater 2018;30(45):e1804130.
[49] Zhang D, Zhong D, Ouyang J, He J, Qi Y, Chen W, et al. Microalgae-based oral microcarriers for gut microbiota homeostasis and intestinal protection in cancer radiotherapy. Nat Commun 2022;13(1):1413.
[50] Seyidoğlu N, Köşeli E, Gurbanlı R, Aydın C. The preventive role of spirulina platensis (arthrospira platensis) in immune and oxidative insults in a stress-induced rat model. J Vet Res 2021;65(2):193–200.